A Wideband Frequency Beam-Scanning Antenna Array for Millimeter-Wave Industrial Wireless Sensing Applications

Abdul Jabbar, *Graduate Student Member, IEEE*, Jalil Ur-Rehman Kazim, *Graduate Student Member, IEEE*, Zhibo Pang, *Senior Member, IEEE*, Muhammad Ali Babar Abbasi, *Senior Member, IEEE*, Qammer Abbasi, *Senior Member, IEEE*, Muhammad Ali Imran, *Fellow, IEEE*, and Masood Ur-Rehman, *Senior Member, IEEE*

***Abstract*—The 57–71 GHz millimeter-wave (mmWave) Industrial, Scientific, and Medical (ISM) band holds significant potential for enhancing the performance of next-generation industrial wireless applications. This paper first presents the design and analysis of a compact and high-performance 8-element series-fed frequency beam-scanning array designed to cover the entire 21.87% fractional bandwidth of the 57–71 GHz ISM band. Using this as a subarray, a hybrid parallel-series feed topology is designed to construct a 64-element (8 × 8) planar array with high-gain directional beams. The planar array provides a peak measured gain of 20.12 dBi at 64 GHz and maintains a flat gain of over 19.23 dBi throughout the band, with a 1 dB gain bandwidth of 13 GHz. Its narrow directional beams provide an average half-power beamwidth of 9.7° and 11.78° in the elevation and azimuth planes, facilitating point-to-point mmWave connectivity and high-resolution beam scanning. The inherent phase variation of the series-fed topology is employed to produce a beamscanning range of 40° within the 57–71 GHz band, with a scan loss of less than 1 dB. The proposed array is a low-cost, and reproducible solution for seamless integration with V-band mmWave equipment, as elucidated through practical demonstration frameworks using mmWave power sensor and EK1HMC6350 evaluation board. The proposed array is well-suited for emerging industrial wireless sensing and imaging applications, and mmWave frequency scanning radars. Its versatility extends to various 60 GHz protocols such as IEEE 802.11ay, IEEE 802.11ad, IEEE 802.15.3c/d, WirelessHD, and other customized industrial protocols such as WirelessHP.**

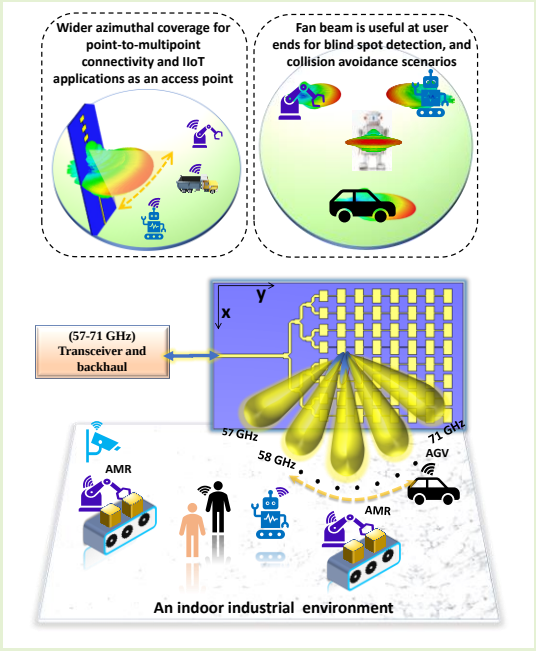

***Index Terms*—60 GHz industrial wireless sensing, frequency beam-scanning, IEEE 802.11ay, radar sensing and imaging.**

I. Introduction

THE next-generation industrial wireless networks require ultra-reliability, extremely low latency, high throughput, and fine-grained spatial differentiation. Traditional wired networks suffer through serious impediments such as expensive installation and maintenance costs, restricted mobility, reduced flexibility, and a lack of reconfigurability in a dynamic industrial environment. Moreover, legacy sub-6 GHz industrial, scientific, and medical (ISM) bands (2.4 and 5 GHz) cannot fully meet the requirements of high speed, high bandwidth (BW), and low latency. In this view, the 60 GHz unlicensed millimeter-wave (mmWave) ISM band is a potential enabler to boost the performance of industrial wireless sensor networks (IWSN) and communication due to its large available BW of 14 GHz from 57 to 71 GHz [1], [2] and compact transceivers/antenna size [3]. The 14 GHz band is divided into six channels, each with 2.16 GHz BW. The channel bonding technique of IEEE 802.11ay supports combining four such channels to extend the bandwidth to 8.64 GHz and link rate to 100 Gbps [4] offering next-generation Wi-Fi. The wide available BW paves the way for a wide variety of indoor industrial wireless applications such as Industrial Internet of Things (IIoT) sensing networks, autonomous mobile robots (AMRs), automated guided vehicles (AGVs), intelligent factory logistics, product tracking through wideband radars, remote visual monitoring and surveillance, image-guided automated assembly, high-definition video and image transmission, fixed wireless access, and high-speed wireless backhaul networks [5]–[8].

Since the mmWave signals propagate in a quasi-optical manner, with the transmitted power reaching the receiver side via line-of-sight (LOS) paths or low-order reflected paths, thus the contribution of diffracted components is insignificant and

(*Corresponding author: Abdul Jabbar*)
Abdul Jabbar, Jalil Ur-Rehman Kazim, Qammer Abbasi, Muhammad Ali Imran, and Masood Ur-Rehman are with James Watt School of Engineering, University of Glasgow, UK (email: abdul.jabbar@glasgow.ac.uk).
Zhibo Pang is with Automation Technology, ABB, Vasteras, Sweden (e-mail: pang.zhibo@se.abb.com).
Muhammad Ali Babar Abbasi is with Center of Wireless Innovation, Queen's University Belfast, UK (e-mail: m.abbasi@qub.ac.uk).

path loss is quite dominant [6]. Additionally, since the oxygen absorption is maximum around 60 GHz, it necessitates the design of high gain antenna arrays to mitigate the undesired path loss as well as to enhance the communication link budget.

At mmWave bands, microstrip printed circuit board (PCB)-based antennas are one of the favoured solutions because of their planar geometry, low cost, ease of fabrication, and ease of integration with radiofrequency (RF) frontends. Several PCB-based mmWave antennas aiming for high gain and compact sizes have been presented in the literature [9]–[15] to list but a few. However, achieving wide impedance BW and high gain flatness over a wide frequency band is quite challenging with microstrip PCB antennas. In [9], a substrate-integrated waveguide (SIW) leaky-wave PCB antenna is reported to cover 55–65 GHz band, however, its gain showed more than 2 dB variations in the band. Moreover, planar SIW antennas require metallized vias which increase the fabrication complexity. In [13], a high-efficiency 60 GHz microstrip antenna was presented but with limited BW and more than 3 dB gain variation in the band of interest. Series-fed microstrip patch arrays provide a compact geometry and simpler feed mechanism at mmWave bands, such as in [14]–[16], but their reported -10 dB reflection BW was lower than 62 GHz with large gain fluctuations in the band. A 60 GHz series-fed antenna array is reported in [15] using Chebyshev tapering distribution, however, its -10 dB impedance BW is limited to 4.2% (58.5 to 62 GHz) with more than 2 dB gain variation in the band. Note that a 3 dB loss (drop) in antenna gain at higher frequencies would mean a 50% loss of power. It is evident that achieving wide antenna BW while maintaining the high flat gain over the entire 60 GHz ISM band with planar microstrip patch-based PCB antennas is quite challenging as well as desirable.

Considering the aforementioned challenges and to fully utilize the potential of 14 GHz of wide available bandwidth around 60 GHz ISM band, we aimed to design a high-performance, wideband, low-cost, and repeatable 60 GHz planar antenna array for next-generation mmWave industrial wireless sensing applications.

The key contributions and achievements of this work are as follows:

- We implemented a new design technique of finite tapering of patch elements in series-fed topology. Contrary to the traditional uniform distribution, binomial distribution, and Chebyshev distribution of series-fed arrays, the proposed finite tapering method significantly enhanced the impedance BW to 41.45 % fractional bandwidth (FBW) covering the entire 21.87% FBW of 57–71 GHz ISM band, while maintaining high flat gain and compact size.
- We significantly simplified the design, emphasizing low-cost considerations to minimize fabrication complexities. This involved avoiding any inset cuts, slots, electroplated vias, additional parasitic patches, or any defective ground structures that could adversely impact or limit RF performance at higher frequencies. Moreover, the microstrip edge-feed technique is employed, providing not only great ease in antenna measurements but also seamless integration with RF circuitry and compatibility with off-the-shelf 1.85 mm standard RF equipment.
- We meticulously designed parallel-series topology for a compact and high gain 64-element array with a total size of 2 cm × 2.8 cm. The planar array offers the peak realized gain of 20.6 dBi at 64 GHz, while the realized gain is above 19.6 dBi within the 57.24–70.2 GHz band. Thus, with a wide -10 dB impedance bandwidth and without sacrificing the gain bandwidth, the proposed array ensures a 1 dB gain bandwidth of 13 GHz, which is the hallmark of the proposed array. This is advantageous to avoid power-hungry and high-cost power amplifiers. Such high-gain performance at higher frequencies is highly desirable to overcome high oxygen absorption and high path loss at the 60 GHz band.
- We exploited the intrinsic phase shifts within the series-fed aperture to exhibit frequency beam-scanning phenomena with the simplest antenna structure. Therefore, the proposed antenna array presents a potential option for various emerging indoor mmWave industrial applications due to its wideband frequency beam-scanning capability. Likewise, in a variety of smart industrial applications as well as frequency scanning mmWave radar systems, it can be employed for sensing and detecting capabilities that may significantly improve the performance of IWSNs.

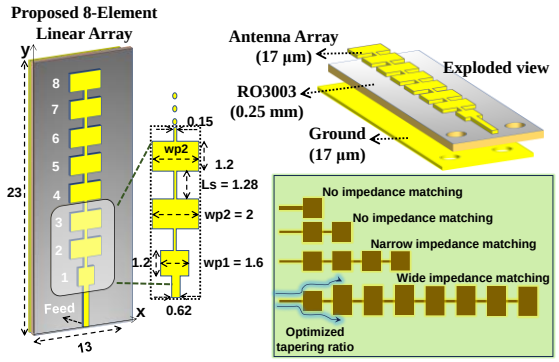

Fig. 1. Schematic design of the proposed 1 × 8 series-fed array (dimensions in mm).

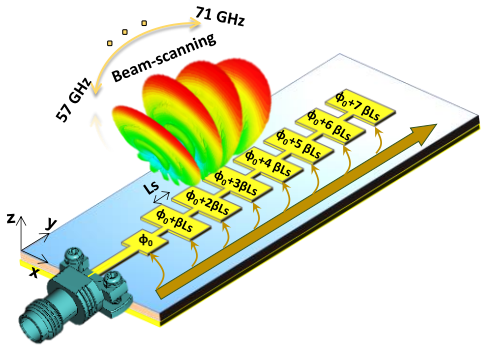

Fig. 2. Illustration of the wave formation across the antenna aperture. The total phase shift along the y-coordinate is contributed by the phase accumulation βLs of the guided wave propagation. The varying net phase relative to the operating frequency results in frequency beam-scanning in the y-z plan.

II. DESIGN AND ANALYSIS OF WIDEBAND LINEAR (1 × 8) ARRAY WITH FAN-BEAM

Microstrip patch antennas are inherently narrowband [17]. Increasing substrate thickness while lowering the quality factor to overcome the narrow BW restriction is one possibility to increase the impedance BW. However, increased surface waves, increased antenna dimensions, and losses would be the cost. Additionally, the stronger surface waves would alter the antenna radiation pattern, interact with other electronics on the same substrate, and potentially affect the feeding structure of the antenna which is not favorable at the 60 GHz band. Therefore, rather than matching a single patch antenna element to a narrow frequency region, we employ the technique of increasing the number of impedance resonances inside the desired band to achieve a wide impedance matching in 57–71 GHz band.

To design a wideband 8-element linear array, optimized finite tapered patch elements are loaded to the first element and connected through a thin series-connected microstrip transmission line (MTL). Thus, our proposed methodology involves two prime aspects, first to tune the antenna with multiple resonances within the band of interest, and second to optimize tapering of elements' width in a way to maintain wide impedance matching with low gain fluctuations over a wide BW. Contrary to the conventional uniform distribution [14], binomial distribution, or Chebyshev distribution [15] of series-fed arrays, the proposed finite tapering method involves the modified and optimized tapering ratio of the first patch as compared to other 7 patch elements (*wp*) loaded to the first patch.

The design philosophy and geometry of the proposed antenna are demonstrated in Fig. 1. We reported a preliminary simulated linear array design in [18] based on Rogers 4003C substrate, however, its gain variation was more than 2.5 dB above 67 GHz with less than 80% radiation efficiency. Nevertheless, in this study, significant contributions were made to improve and maintain consistent antenna performance up to 71 GHz. This included investigating and validating frequency beam-scanning capabilities, subsequently developing a compact high-performance 64-element planar antenna array, and conducting rigorous measurements in 60 GHz band to verify the prototype.

The proposed antenna is designed using Rogers 3003 laminate substrate with a dielectric constant of 3, a loss tangent of 0.001, a dielectric thickness of 0.25 mm, and a copper thickness of 18 µm. Initially, a quarter-wavelength patch with a length of 1.2 mm (less than $\lambda_0/4$ to accommodate fringing effects) and a width (wp_1) of 1.6 mm. A full ground plane was used at the bottom of the substrate to achieve a broadside radiation pattern. Microstrip edge-feed is designed at 50 Ohm for ease of measurement and seamless integration, as depicted in Fig. 2 with the connector model.

Contrary to the conventional uniform distribution, binomial distribution, or Chebyshev distribution [15], the tapering of the other 7 patches (patches 2 to 8) was optimized to 2 mm (instead of 1.6 mm width of patch 1), here termed as finite tapering. The input impedance of each patch is loaded with the series-fed MTL and the patch next to it, which varies with operating frequency. Initially, the impedance of the single patch element was found to be around 210 Ω.

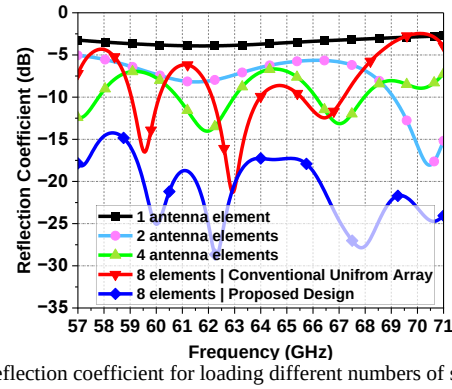

Fig. 3. Reflection coefficient for loading different numbers of series-fed patch antenna elements (1, 2, 4, and 8 elements).

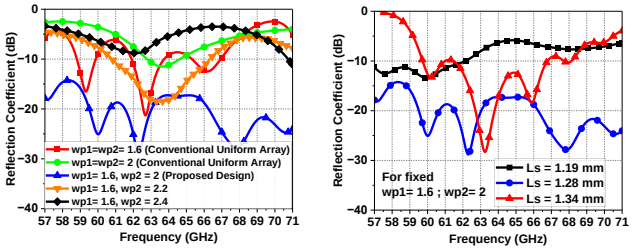

Fig. 4. (a) Effect of width tapering on -10 dB impedance BW of the proposed 1 × 8 array (b) Effect of change in the length of series-connecting MTL array.

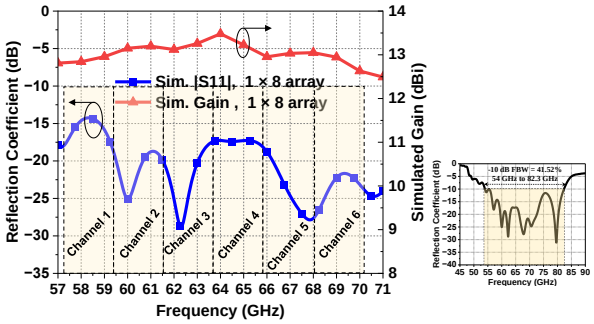

Fig. 5. Simulated reflection coefficient and realized gain of the proposed 1 × 8 sub-array covering all 6 channels of 60 GHz band. The miniaturized figure shows a full range reflection coefficient revealing 41.52% FBW.

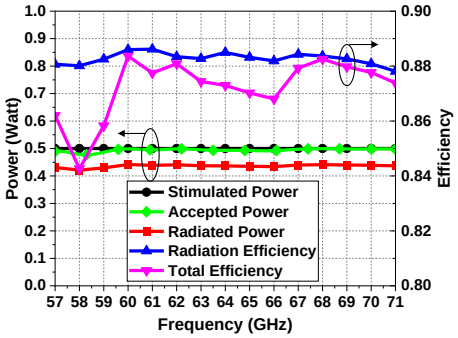

Fig. 6. Simulated power profile, radiation efficiency, and total efficiency of the proposed 1 × 8 array.

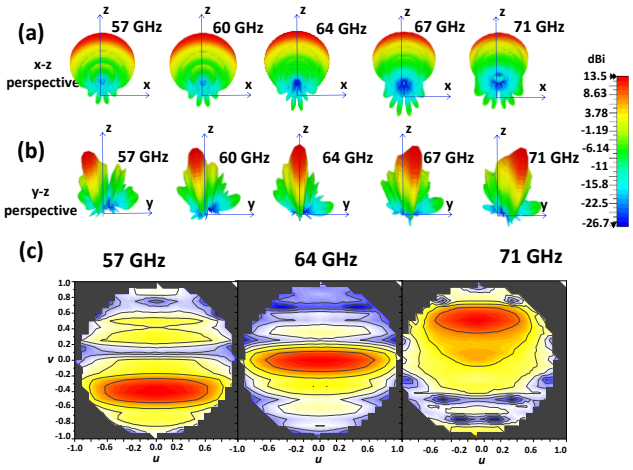

Fig. 7. (a and b) 3-D simulated radiation patterns of the proposed 1 × 8 array in 57–71 GHz band from two different angular perspectives. Fan-beam can be observed with wider beamwidth in one plane. (c) The u-v orthographic projection reveals frequency beam-scanning performance.

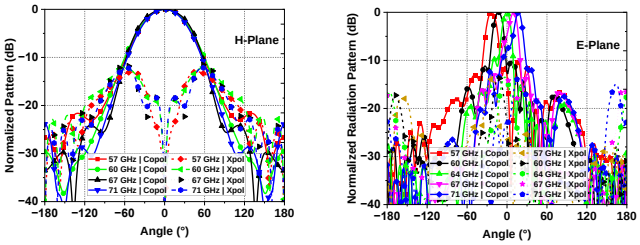

Fig. 8. Rectangular plots of simulated radiation patterns of the proposed 1 × 8 array across 57–71 GHz band. (a) x-z plane (phi 0°). (b) y-z plane (phi 90°).

By loading the initial patch element to the seven other optimized patches and seven optimized MTLs, the impedance characteristics of each patch element change, including varying phases. This design methodology leads to the emergence of different resonant modes in close spectral proximity, such as at 57.1, 60.04, 62.31, 67.81, and 70.61 GHz in case of the proposed array design as illustrated in Fig. 3. Consequently, the antenna array achieves a broad -10 dB impedance matching, while achieving an overall average input impedance of 50 Ω. The series MTL has an optimized width of 0.15 mm (must be within fabrication limits) and a length (*Ls*) of 1.28 mm.

It is evident from Fig. 3 that with all identical patch elements (i.e., the case of the uniformly distributed array), -10 dB impedance BW is limited with few resonance points. Similarly, as tapering was increased towards the center of the array (i.e., wp_2 = 2.2, 2.4, 2.6 mm which tends to be the case of binomial/Chebyshev distribution), the BW becomes quite smaller (less than 2 GHz) with reduced flat gain and also leads to increased size of patch elements. However, with the proposed design approach of finite tapering, the entire 57–71 GHz band is covered.

The effect of the tapering width (wp_2) of the patch elements and length (*Ls*) of the series-connected MTL on impedance BW is shown in Fig. 4(a) and (b) respectively. Note that in Fig. 4(a), the curves for wp_1=wp_2 correspond to all identical elements including the first patch element, which becomes the case of a conventional uniform distributed array and shows limited BW and high gain fluctuation.

The optimized simulated reflection coefficient (-10 dB impedance BW) and realized gain of the proposed 1 × 8 array are shown in Fig. 5. The -10 dB impedance BW is 54–82.3 GHz covering all 6 channels of the 60 GHz ISM band. It provides a peak gain of 13.48 dBi at 64 GHz. The realized gain is above 12.36 dBi in 57–71 GHz, thereby providing less than 1 dB gain variation in the desired band of interest. As shown in Fig. 6, for an input stimulated signal of 0.5 W, the accepted power is above 0.477 W throughout 57–71 GHz. The radiated power varies between 0.421 W to 0.441 W, which results in above 87.81% radiation efficiency and above 84.26% total efficiency in the whole 57–71 GHz band. Note that radiation efficiency is the ratio of the radiated power to the accepted power, whereas total efficiency is the ratio of the radiated power to the input stimulated power which also accounts for losses due to mismatch.

The 3-D radiation patterns at various frequency points are shown in Fig. 7(a) and (b). A fan-shaped radiation pattern is observed with a wider half-power beamwidth (HPBW) in x-z -plane (phi 0°) ranging between 63.44° to 77° across 57-71 GHz band, as shown in Fig. 7(a) and Fig. 8(a). A relatively narrow HPBW is achieved in y-z plane (phi 90°) ranging between 12° to 14°, as shown in Fig. 7(b) and Fig. 8(b). This is due to the linear geometry of the array in which the radiation pattern is squeezed along the direction of elements while expanding in the orthogonal direction. The array is broadside at 64 GHz. The side-lobe levels (SLL) are below -10 dB in both planes with very low (x-pol) levels in the direction of the main beam, as revealed in Fig. 8.

The fan beam pattern is advantageous in point-to-multipoint connectivity in various indoor mmWave wireless industrial applications which include sensing and monitoring industrial processes for data collection and proactive analysis, predictive maintenance, asset tracking, and collision avoidance [19]–[22]. Moreover, the proposed wideband 60 GHz array is advantageous to cover a wide sectoral region for efficient energy transport over 60 GHz for IWSN [23]. The array is linearly polarized. A linear polarized antenna typically exhibits lower cross-polarization levels, as verified in Fig. 8. This means it can provide better discrimination between the desired signal and unwanted signals with different polarization. Moreover, the linear polarized antennas may experience reduced multipath interference compared to circular polarized antennas. This is particularly beneficial in environments with strong reflective surfaces, such as harsh industrial environments.

III. Frequency Beam-Scanning Analysis

The variation in the main beam direction with frequency is created by the analog phase shifts that apply the same phase shift for signals at different frequencies. When the signal bandwidth is large, the fixed antenna spacing in the series-fed topology induces frequency-dependent phase shifts across the array, causing the frequency-dependent beam-scanning phenomenon, as shown in Fig. 2. The phase variation along the series-fed elements at each operating frequency acts as ϕ, $\phi+\beta Ls$, $\phi+2\beta Ls$,… , $\phi(n-1)\beta Ls$, where ϕ is the reference phase at the first element and *n* is a total number of elements of the

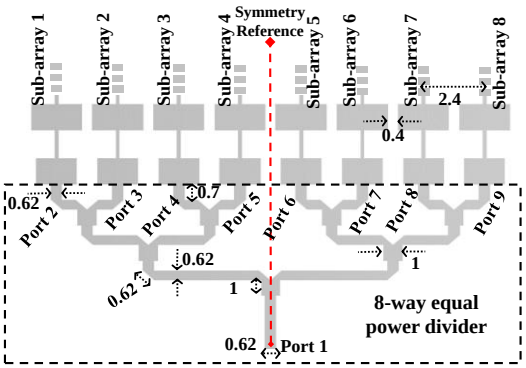

Fig. 9. Schematic design of 8-way equal power divider to excite 8 sub-arrays in a parallel-series topology (dimensions in mm).

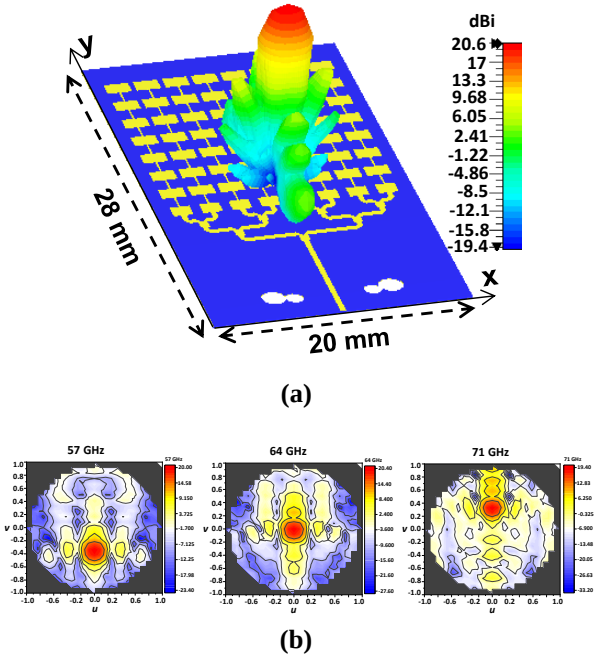

Fig. 10. (a) 3-D simulated schematic design of the proposed planar array with broadside beam at 64 GHz. (b) u-v heat maps at start, mid, and end frequencies demonstrating beam-scanning.

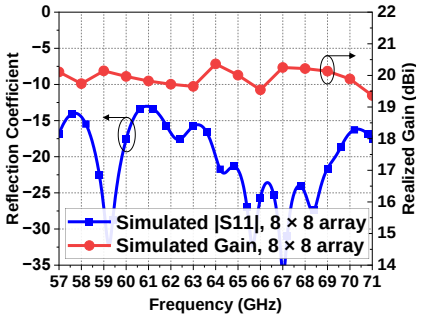

Fig. 11. Simulated reflection coefficient and realized gain of the proposed 8 × 8 array.

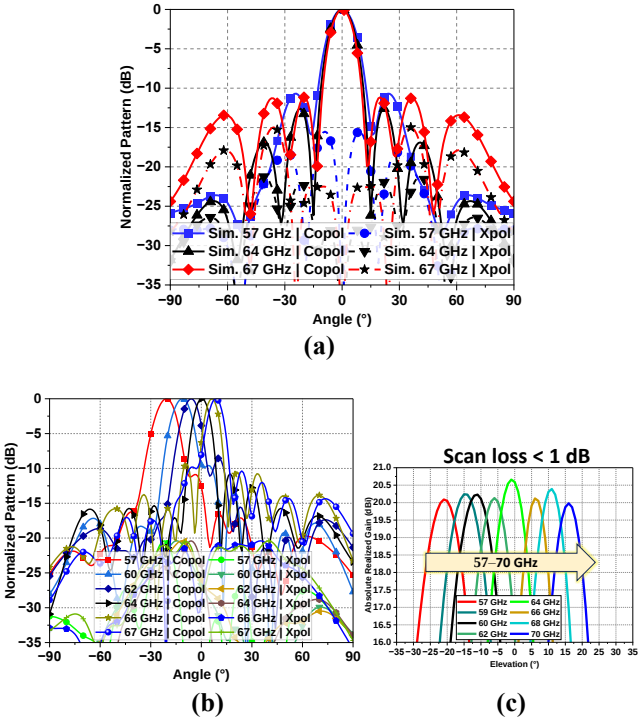

Fig. 12. Simulated radiation patterns of 8 × 8 array at various operating frequency points. (a) in x-z plane. (b) in y-z plane. (c) un-normalized realized gain pattern in the y-z plane illustrating scan loss of less than 1 dB.

array. In fact, βLs is the electrical length that adds a phase shift along the direction of the array. Here, $\beta=2\pi/\lambda_g$ is the phase constant of the propagation wave and is a frequency-dependent parameter. It indicates how the phase of the wave changes as it travels through a medium. *Ls* represents the length of the path (MTL) over which the wave propagates. For each operating frequency, the parameter β alters, leading to a change in the total accumulated phase across the antenna aperture at that frequency. Thus, the total phase shift along the y-coordinate (where elements are arranged in series) is contributed from the phase accumulation βLs of the wave propagation which results in the frequency beam-scanning phenomenon. The u-v heat maps in Fig. 7(c) reveal that the main beam shifts in the elevation plane with the change in operating frequency, making it adaptable to changing communication or sensing requirements.

IV. Design and Analysis of 8 × 8 Planar Array

The high gain of the antenna array translates into a reduction of the transmit power needed for a given link performance and enhances signal-to-noise ratio (SNR) at the receiver end. Thus, in a harsh industrial environment, the high gain array at 60 GHz is crucial to mitigate path loss and facilitates reliable connectivity over a distance of tens of meters. To design a compact and high-gain array, an 8-channel equal power divider is designed and integrated with eight of the proposed linear sub-arrays at each output port of the divider, as shown in Fig. 9. In this way, each proposed 1 × 8 array acts as a sub-array to design a compact 64-element (8 × 8) planar array.

The consistency in the magnitude and phase of the transmission coefficients of a power divider is crucial for the reliable transmission of data packets for accurate delivery of signals to the nodes of industrial access networks [24].

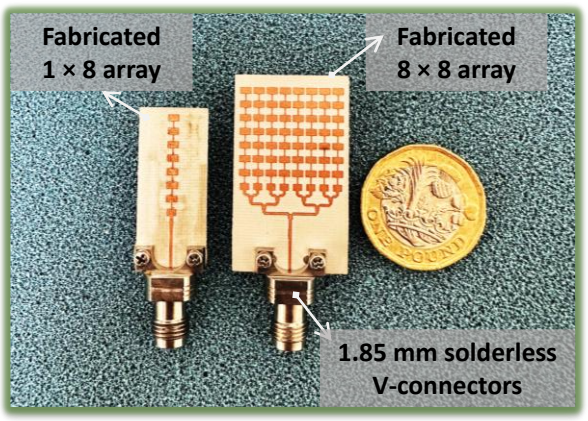

Fig. 13. Fabricated prototypes of the proposed 60 GHz antenna arrays.

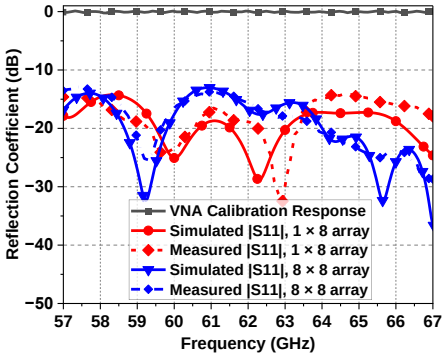

Fig. 14. Measured reflection coefficient of the proposed 1 × 8 and 8 × 8 arrays.

The insertion loss of the power divider is within -9.6 to -10.1 dB, whereas the reflection coefficient (|S11|) is maintained to be less than -10 dB within the desired band (not shown here due to brevity). The 3-D schematic view of the proposed 64-element (8 × 8) array is shown in Fig. 10(a), whereas Fig. 10(b) reveals heat maps demonstrating the frequency beam-scanning.

The simulated reflection coefficient and realized gain are shown in Fig. 11. The array provides a peak simulated realized gain of 20.66 dBi at 64 GHz. In contrast, the simulated realized gain is above 19.71 dBi in 57–70.5 GHz band. A high gain flatness is achieved with a 1 dB gain BW of 13 GHz. The 2-D radiation patterns in x-z and y-z planes are shown in Fig. 12 (a and b). High-gain directional radiation patterns with narrow beamwidth in both azimuth and elevation planes are achieved. Within 57–70.5 GHz, the simulated HPBW varies between 10.87° to 13.14° in the azimuth plane and 7.86° to 10.98° in the elevation plane. The sidelobe levels are below -10 dB, and the x-pol levels in the direction of the main beam are below -20 dB. The radiation efficiency of the 8 × 8 array is above 83 % in 57–71 GHz band. The scan loss across frequency-beam scanning over 57–71 GHz is less than 1 dB, as shown in Fig. 12(c). The achieved scanning rate is 1.82°/FBW. The scanning rate is the ratio of the scanning range to the FBW [25].

V. Prototype Fabrication and Measurement Result

The fabricated prototypes of the proposed 1 × 8 (sub-array) and 8 × 8 (64-element) arrays are shown in Fig. 13. The size of the 8 × 8 array including the power divider is 20 mm (4 λ_0) × 28 mm (5.6 λ_0) × 0.25 mm (0.05λ_0), where λ_0 is free space wavelength at 60 GHz. To excite the antenna array, an edge-launched reusable solderless 1.85 mm standard V-connector was used. As soldering is not required in this type of connector, the loss due to the copper deposition during the soldering process is hence avoided.

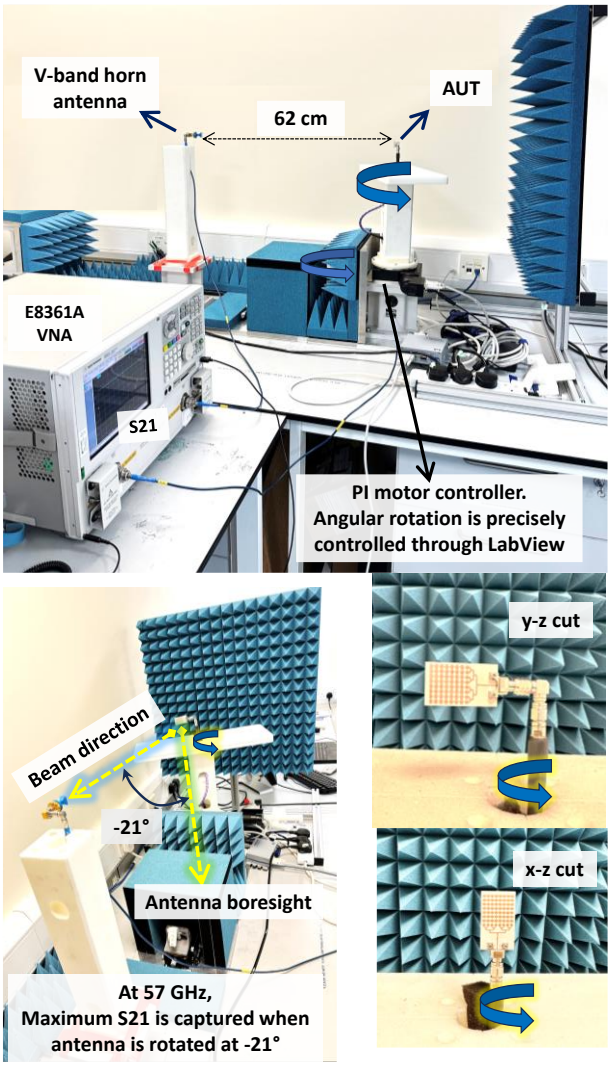

Fig. 15. 60 GHz OTA measurement setup to test the radiation patterns and gain in an open indoor laboratory environment.

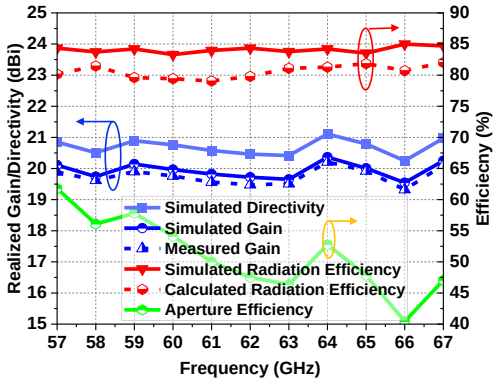

Fig. 16. Measured gain, calculated radiation efficiency, and aperture efficiency of the proposed 8 × 8 array.

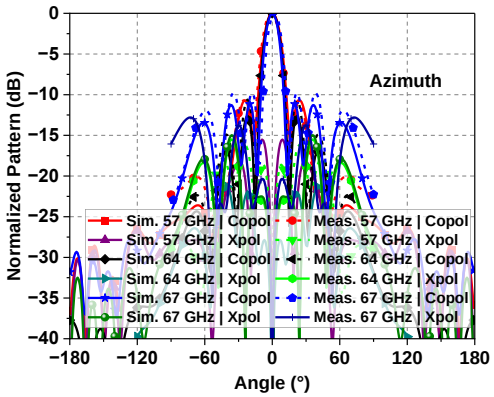

Fig. 17. Measured radiation patterns of 8 × 8 array at 57, 64, and 67 GHz in x-z plane.

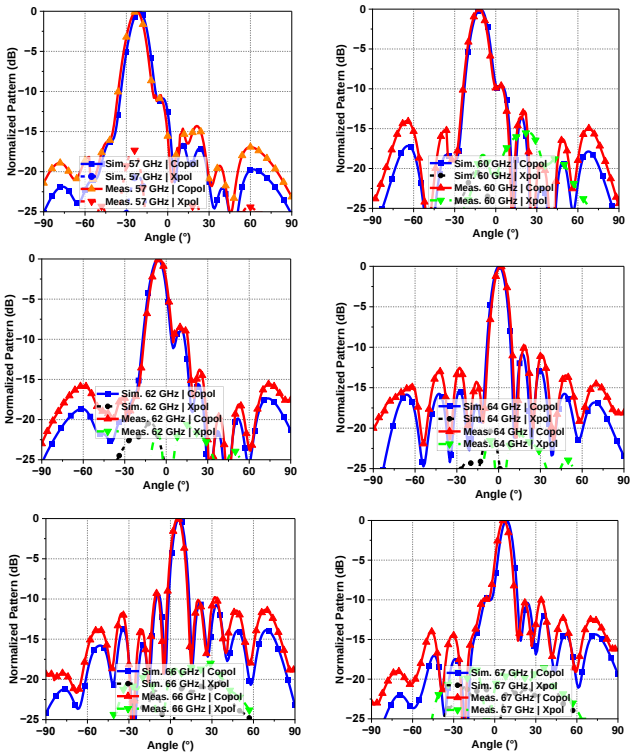

Fig. 18. Measured radiation patterns of 8 × 8 array at 57, 60, 62, 64, 66, and 67 GHz in y-z plane.

launched reusable solderless 1.85 mm standard V-connector was used. As soldering is not required in this type of connector, the loss due to the deposition of copper during the soldering process is avoided (as it might adversely affect the performance at 60 GHz). Here, it is instructive to mention that we utilized 1.85 mm standard RF equipment in our measurement setup, which supports a maximum frequency of 67 GHz. Consequently, the measured results are presented here within 57–67 GHz range. The reflection coefficients (i.e., -10 dB impedance BW) of the proposed 1 × 8 and 8 × 8 arrays were measured using an Agilent E8361A vector network analyzer (VNA). Measured results match reasonably well with the simulations, as shown in Fig. 14. Small discrepancies are mainly due to fabrication tolerance and surface roughness.

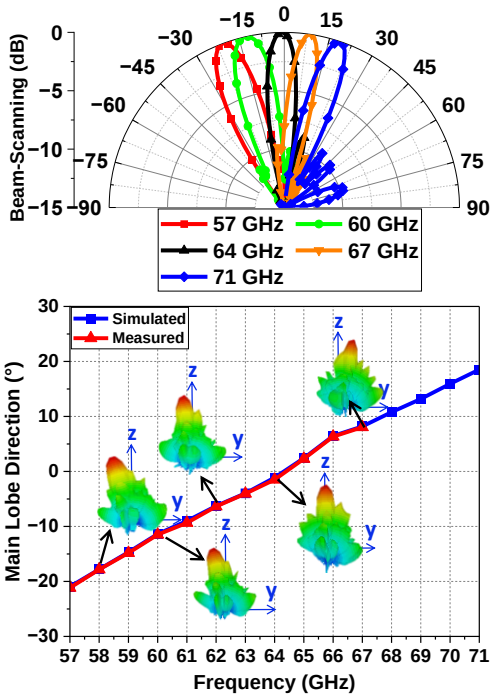

Fig. 19. Measured frequency beam-scanning performance of 8 × 8 array in y-z plane (up to 67 GHz) demonstrated in polar form (top) and 3-D pattern visualization with the main lobe direction (bottom). The blue curve shows the simulated result.

TABLE I.
PERFORMANCE COMPARISON OF THE PROPOSED WORK WITH CLOSELY RELATED 60 GHZ ANTENNAS

Ref.	Array Type and Geometry	-10 dB BW (FBW %)	Peak Gain (dBi)/ Gain Variation in 57-71 GHz	Beam-scanning (Scanning Range)	Size (mm) (W × L × H) *(*λ=5mm at 60 GHz)*
[9]	SIW planar leaky wave slot array 1 × 8	55–65 (16.66 %)	14.5 (> 3 dB)	Yes -72° to +48°	23 × 38 × 0.38 (4.6λ×7.6λ×0.076)
[10]	Planar SIW slot array 12 × 12	59.3–61.8 (4.12 %)	22 (> 3 dB)	No	NA × NA × 0.51 (*λ ×*λ× 0.102λ)
[11]	SIW multilayer PCB 1 × 4	50.79–70.85 (33 %)	11.9 (> 3 dB)	No	22 × 25 × 1.05 (4.4λ×5λ×0.21λ)
[12]	Series-fed microstrip patch array 1 × 4	57–66 (14.63%)	14.5 (< 1 dB)	No	14.7 × 6 × 0.25 (2.94λ×1.2λ×0.04)
[13]	Microstrip dipoles 1 × 4	57–64 (10.69 %)	16.5 (> 3 dB)	No	18.5 × 30 × 0.25 (3.7λ×6λ× 0.05λ)
[14]	Parallel-series fed microstrip patch array 8 × 4	58–60.5 (4.22%)	18 (Not given)	No	35 × 35 × 0.1 (7λ×7λ× 0.02λ)
[15]	Series-fed microstrip patch array 2 × 10	58.5–62 (4.2%)	16.4 (> 3 dB)	Partial, at two angles only. -20° and +20	× 30 × 0.51 (3.7λ×6λ× 0.102λ)
This Work	**Series-fed linear array 1 × 8**	**54–82.3 (41.52%, sim.) 54–67 (meas. presented)**	**13.48 (< 1 dB)**	**Yes -23° to +17°**	**13 × 23 × 0.25 (2.6λ×4.6λ×0.05λ)**
	Parallel-series planar array 8 × 8	**49.28–73 (38.79%, sim.) 49.28–67 (meas. presented)**	**20.36 (< 1dB)**	**Yes -21° to +19°**	**20 × 28 × 0.25 (4λ×5.6λ×0.05λ)**

An over-the-air (OTA) antenna measurement setup was prepared in an open space of an indoor lab environment to measure far-field radiation pattern and gain, as shown in Fig. 15. A complete anechoic chamber is not needed for 60 GHz measurements due to directional characteristics and high path loss at this band. Note that this feature stands out as a key advantage of mmWave bands, contributing to the inherent security of critical mmWave industrial communication. A standard gain V-band horn antenna was used as a transmitter (Tx), whereas the proposed array under test (AUT/Rx antenna) was mounted on a 360° rotator/turntable. The turntable is attached to a PI motor controller and the rotation was automated using LabVIEW with a precise angular resolution of 1° step.

The distance between the Tx and Rx antennas was set as 62 cm to satisfy the far-field condition. If the distance between Tx and Rx antennas is increased, then the normalized radiation patterns would still be similar. However, the absolute received power level/S21 level will decrease according to the Friis equation [17] , because the path loss will increase, as varies in direct proportion with the square of the distance (d) between Tx and Rx antennas as: $Path\ loss\ = 20 \times \log(4\pi d/\lambda)$.

The array gain was measured using the relative gain comparison method. Two sets of measurements were performed at each frequency at a single direction of maximum power with a 1 GHz step in 57–67 band and S21 was measured on VNA. In one set, S21 was measured using two identical horn antennas ($S_{21_{horn}}$), whereas, in the other set, one of the horns was replaced with the proposed array ($S_{21_{array(dB)}}$). At each test frequency, the gain (in dB scale) was calculated by $G_{array_{(dB)}} = G_{horn_{(dB)}} + S_{21_{array(dB)}} - S_{21_{horn(dB)}}$,where G_{array} is the measured gain of the array at a fixed frequency and G_{horn} is the known gain of the standard gain horn antenna at that frequency. The measured gain, directivity, and radiation efficiency of the proposed 8 × 8 array are shown in Fig. 16. The peak measured gain is 20.12 dBi at 64 GHz. The measured gain is above 19.23 dBi throughout the band of interest, thereby providing a measured 1 dB gain-BW of more than 13 GHz. The calculated radiation efficiency was found using the measured gain as: $Cal.Rad.Eff. = \frac{Measured\ Gain}{Simulated\ Directivity}$. The peak aperture efficiency of 8 × 8 array is 61.79% at 57 GHz. Aperture efficiency is a measure of how effectively the antenna's physical area is used. At each operating frequency, the aperture efficiency was calculated using measured gain and effective physical area ($W \times L$) of 8 × 8 array, excluding power divider ($Aperture\ Efficiency\ = \frac{Gain_{measured} \times \lambda^2}{4\pi \times W \times L}$).

The radiation patterns were measured in both azimuth and elevation planes in 1° resolution from -90° to +90°. The measured radiation pattern in the x-z plane (phi 0° of simulated reference) at 57, 64, and 67 GHz is shown in Fig. 17 which matches quite well with the simulated results. The SLLs are below -10 dB and x-pol levels are below -30 dB in the direction of the main lobe. The radiation pattern in the y-z plane in 57-67 GHz range was measured by rotating the array as well as horn to 90° as shown in Fig. 15. Measured radiation patterns in the y-z plane are shown in Fig. 18, which is the principal plane of beam-scanning because the elements' arrangement is along the y-axis. The measured HPBW ranges between 8.1° to 10.8° from 57–67 GHz in the y-z plane. SLL is less than -10 dB and x-pol levels are below -20 dB. Another visualization of the measured frequency beam-scanning performance of the proposed 8 × 8 array in the y-z plane in polar form along with 3D beams' direction is demonstrated in Fig. 19.

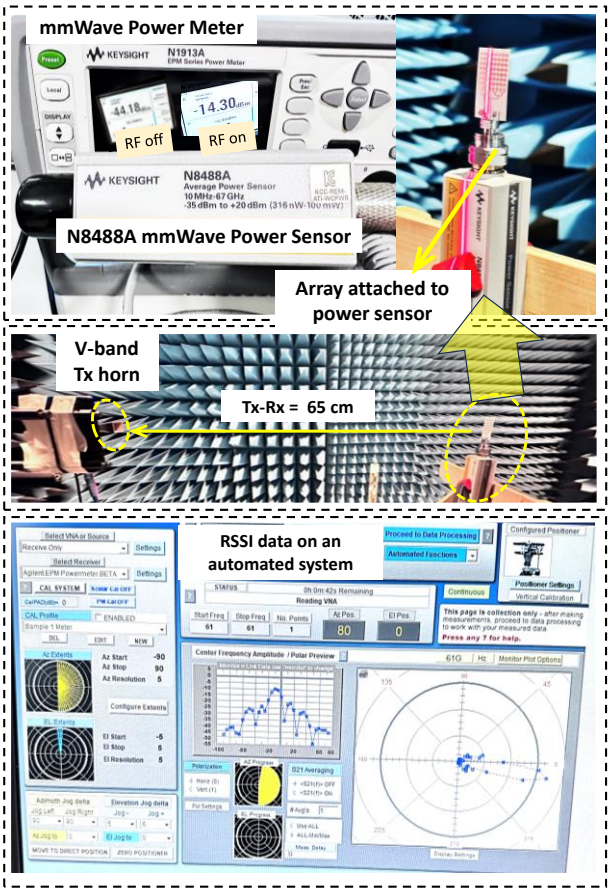

Fig. 20. RF sniffing to capture RSSI with the proposed antenna array in 60 GHz band using N8488A mmWave power sensor.

Table I compares the performance of the proposed array design with other closely related antenna arrays at 60 GHz band in the literature. It can be noticed that the proposed array outperforms various other designs in terms of high-performance indicators such as wide impedance BW, and high flat gain while maintaining a compact size.

VI. Practical Application Scenarios of the Proposed Antenna Array: RF Sensing and Integration with Standard 60 GHz Equipment

The commercially available standard high-frequency V-band antennas (such as standard gain horn antennas) are often extremely costly as well as bulky. The proposed planar antenna array presented in this work offers a tremendously low-cost, compact, and reproducible solution with cheap planar fabrication techniques such as PCB milling. Moreover, the proposed array offers comparable and satisfactory performance in terms of gain and bandwidth, with wide beamwidth coverage (in case of linear 1 × 8 array) as well as highly directional narrow beams (in case of 8 × 8 array). Here, we briefly demonstrate two use cases of the proposed array for 60 GHz sensing applications.

A. RF Sensing and RSSI Test

To test the usability and RF sensing performance of the proposed 60 GHz array prototype, we demonstrate two basic test scenarios with 8 × 8 planar array. The seamless integration with 1.85 mm standard mmWave equipment is easily achievable due to the design of the edge-fed microstrip feed. First, we conducted RF sniffing to capture the received signal strength indicator (RSSI) at a distance of 65 cm between a Tx horn and the proposed array as Rx antenna. The test setup is demonstrated in Fig. 20. The proposed array was attached with Keysight's N8488A mmWave power sensor. The output of the power sensor was connected to the N1913A mmWave power meter. A CW RF signal was generated using a mmWave signal generator at different frequencies and RSSI was analyzed. The dynamic range of about 30 dB was achieved without using any power amplifier. At 60 GHz for instance, the peak received power level was -14.30 dBm, whereas it was below -44.18 dBm when RF was switched off from the RF generator. Such RSSI-based measurements can be employed to analyze radio propagation scenarios, implement channel sounding techniques, characterize the RF performance in terms of transmitted Effective Isotropic Radiated Power (EIRP), as well as to model the path loss of different types of indoor industrial environments within 60 GHz band.

B. Demonstration of 60 GHz Wireless Link Using Proposed Array With EK1HMC6350 Evaluation Board and HMC 6300/6301 Transmit/Receive Chipsets

Owing to the directional features of 60 GHz antennas and numerous sensing and detection applications as well as joint communication and sensing for autonomous vehicles scenarios using signal processing evaluation platforms have been demonstrated earlier [26]–[29]. However, expensive mmWave V-band horn antennas are often used to establish a working setup. Our proposed antenna array provides an off-the-shelf and low-cost solution to test various sensing scenarios using 60 GHz signal processing and evaluation platforms.

Here, we briefly demonstrate a direct integration of our proposed array with Analog Devices EK1HMC6350 evaluation kit to establish a 60 GHz mmWave link. The experimental setup is demonstrated in Fig. 21. It includes an HMC6300 chipset with the Tx module and an HMC6301 with the Rx module, a USB interface, and a graphical user interface (GUI) to program the Tx and Rx chipsets by writing to the device registers. Two evaluation boards were used for separate Tx and Rx chipsets being half-duplex systems.

To test the setup, a 1 MHz FM signal was supplied to the evaluation board which is upconverted in the 57 to 64 GHz range. The transmitter was locked at 60 GHz through Tx and Rx GUIs. First, a 1.85mm standard coaxial cable was attached between Tx and Rx boards to ensure the proper working of boards and signal retrieval, as illustrated in Fig. 21(a). Then, the coaxial cable was replaced by the proposed 8 × 8 planar arrays to confirm the 60 GHz wireless link. A 4-channel oscilloscope was used to observe the transmitted and received signal waveforms. The transmitted waveform was successfully received. We conducted a Tx-Rx link test using two identical 8 × 8 arrays, one at the Tx side and the other at the Rx side. Additionally, for verification, we replaced one of the arrays with a commercial V-band horn antenna, as shown in Fig. 21(b). The received waveform was similar in both instances. Such demonstration platform when used with digital baseband processing can be used to analyze bit error rates, error vector magnitude, as well as other link budget analyses. Moreover, as illustrated in Fig. 21(c), the received signal is blocked (flat line on the oscilloscope) when LOS is blocked by placing a hand in between the Tx and Rx antennas. This type of blocking effect provides an efficient signature in the 60 GHz sensing domain and can be employed for 60 GHz activity monitoring and sensing in indoor environments.

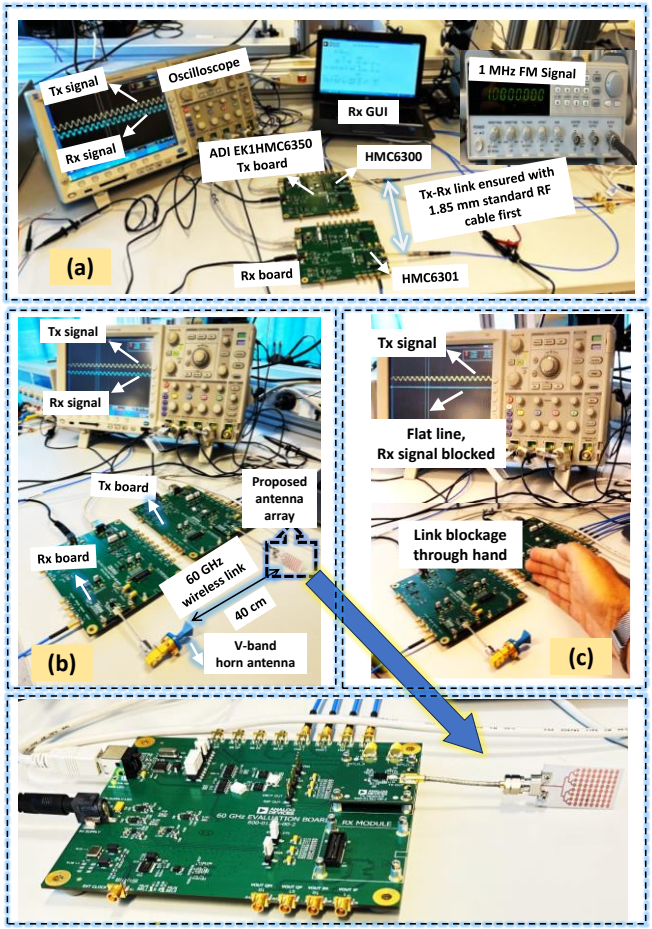

Fig. 21. Demonstration of establishing a 60 GHz wireless link using the proposed antenna array with Analog Devices EK1HMC6350 evaluation board. (a) end-to-end signal transfer using 1.85 mm coaxial cable (b) 60 GHz wireless signal transfer using the proposed antenna array. (c) effect of hand blockage.

VII. Conclusion

In this paper, the design of a compact and wideband planar antenna array is presented for the 57–71 GHz ISM band, featuring a high gain and frequency beam-scanning capability of 40°. Employing eight linear arrays as sub-arrays, a planar 64-element (8 × 8) array is developed with a hybrid parallel-series topology, demonstrating a peak realized gain of 20.12 dBi at 64 GHz and less than 1 dB gain variation across 57–70 GHz, with a compact size of 2 cm × 2.8 cm. The directional beams make

it suitable for secure point-to-point multi-Gbps links. Experimental validations confirm the antenna performance and verify frequency beam-scanning performance with a scan range of 40° within 57–71 GHz and scan loss of less than 1 dB. Using the proposed antenna array, a practical demonstration of RF sensing for RSSI sensing as well as establishing a 60 GHz mmWave wireless link with Analog Devices EK1HMC6350 evaluation is presented. and HMC6300/6301 chipsets. The performance of the proposed prototype showed considerable advantages over various other proposed V-band antennas in terms of size, wide bandwidth, high flat gain, efficiency, and beam-scanning with the simplest antenna structure. The proposed array offers a low-cost, compact, and wideband solution for seamless integration with 60 GHz mmWave frontends. It is beneficial to build and test mmWave IWSN as well as wideband frequency beam-scanning radars for sensing, collision avoidance, and mmWave imaging.

REFERENCES

[1] Z. Pang, M. Luvisotto, and D. Dzung, "Wireless high-performance communications: The challenges and opportunities of a new target," *IEEE Ind. Electron. Mag.*, vol. 11, no. 3, pp. 20–25, 2017.

[2] S. Saponara, F. Giannetti, B. Neri, and G. Anastasi, "Exploiting mm-wave communications to boost the performance of industrial wireless networks," *IEEE Trans. Ind. Informatics*, vol. 13, no. 3, pp. 1460–1470, 2017.

[3] R. Jacobi and A. Aginskiy, "Choosing 60-GHz mmWave sensors over 24-GHz to enable smarter industrial applications," *Nov 2018, Texas Instruments*, 2018.

[4] Y. Ghasempour, C. R. C. M. Da Silva, C. Cordeiro, and E. W. Knightly, "IEEE 802.11 ay: Next-generation 60 GHz communication for 100 Gb/s Wi-Fi," *IEEE Commun. Mag.*, vol. 55, no. 12, pp. 186–192, 2017.

[5] A. Mahmood *et al.*, "Industrial IoT in 5G-and-beyond networks: Vision, architecture, and design trends," *IEEE Trans. Ind. Informatics*, vol. 18, no. 6, pp. 4122–4137, 2021.

[6] M. Cheffena, "Industrial wireless communications over the millimeter wave spectrum: opportunities and challenges," *IEEE Commun. Mag.*, vol. 54, no. 9, pp. 66–72, 2016.

[7] E. Sisinni, A. Saifullah, S. Han, U. Jennehag, and M. Gidlund, "Industrial internet of things: Challenges, opportunities, and directions," *IEEE Trans. Ind. Informatics*, vol. 14, no. 11, pp. 4724–4734, 2018.

[8] A. Jabbar *et al.*, "Millimeter-Wave Smart Antenna Solutions for URLLC in Industry 4.0 and Beyond," *Sensors*, vol. 22, no. 7, p. 2688, 2022, doi: 10.3390/s22072688.

[9] A. Sarkar and S. Lim, "60 GHz compact larger beam scanning range PCB leaky-wave antenna using HMSIW for millimeter-wave applications," *IEEE Trans. Antennas Propag.*, vol. 68, no. 8, pp. 5816–5826, 2020.

[10] X.-P. Chen, K. Wu, L. Han, and F. He, "Low-cost high gain planar antenna array for 60-GHz band applications," *IEEE Trans. Antennas Propag.*, vol. 58, no. 6, pp. 2126–2129, 2010.

[11] J. Zhang, X. Zhang, and A. A. Kishk, "Broadband 60 GHz antennas fed by substrate integrated gap waveguides," *IEEE Trans. Antennas Propag.*, vol. 66, no. 7, pp. 3261–3270, 2018.

[12] T. H. Jang, H. Y. Kim, I. S. Song, C. J. Lee, J. H. Lee, and C. S. Park, "A wideband aperture efficient 60-GHz series-fed E-shaped patch antenna array with copolarized parasitic patches," *IEEE Trans. Antennas Propag.*, vol. 64, no. 12, pp. 5518–5521, 2016.

[13] Y. Al-Alem and A. A. Kishk, "Efficient millimeter-wave antenna based on the exploitation of microstrip line discontinuity radiation," *IEEE Trans. Antennas Propag.*, vol. 66, no. 6, pp. 2844–2852, 2018.

[14] J. Säily, A. Lamminen, and J. Francey, "Low cost high gain antenna arrays for 60 GHz millimetre wave identification (MMID)," in *Sixth ESA Workshop on Millimetre-Wave Technology and Applications-Fourth Global Symposium Millimetre Waves, Espoo, Finland*, 2011.

[15] Y. Liu *et al.*, "Design and fabrication of two-port three-beam switched beam antenna array for 60 GHz communication," *IET Microwaves, Antennas \& Propag.*, vol. 13, no. 9, pp. 1438–1442, 2019.

[16] A. Attaran, R. Rashidzadeh, and R. Muscedere, "Rotman lens combined with wide bandwidth antenna array for 60 GHz RFID applications," *Int. J. Microw. Wirel. Technol.*, vol. 9, no. 1, pp. 219–225, 2017.

[17] C. A. Balanis, *Antenna theory: analysis and design*. John wiley & sons, 2015.

[18] A. Jabbar, Z. Pang, G. A. Safdar, Q. Abbasi, M. A. Imran, and M. Ur-Rehman, "A Compact Wideband Millimeter-Wave Beam-Scanning Antenna Array for Industry 4.0 and Beyond Applications," *2023 IEEE Int. Work. Antenna Technol.*, pp. 1–4, 2023.

[19] K. Z. Ghafoor *et al.*, "Millimeter-wave communication for internet of vehicles: status, challenges, and perspectives," *IEEE Internet Things J.*, vol. 7, no. 9, pp. 8525–8546, 2020.

[20] L. Lu, X. Ma, Y. Liang, Z. Liu, X. Fan, and L. Li, "A 60-GHz Hybrid FMCW-Doppler Radar for Vibration Detection With a Robust I/Q Calibration Method," *IEEE Sens. J.*, vol. 22, no. 21, pp. 20464–20474, 2022.

[21] Z. Briqech, S. Gupta, A.-A. Beltay, A. Elboushi, A.-R. Sebak, and T. A. Denidni, "57--64 GHz imaging/detection sensor—Part II: Experiments on concealed weapons and threatening materials detection," *IEEE Sens. J.*, vol. 20, no. 18, pp. 10833–10840, 2020.

[22] M. Rameez, M. I. Pettersson, and M. Dahl, "Interference Compression and Mitigation for Automotive FMCW Radar Systems," *IEEE Sens. J.*, vol. 22, no. 20, pp. 19739–19749, 2022.

[23] H. Li, K. Ota, M. Dong, and H.-H. Chen, "Efficient energy transport in 60 GHz for wireless industrial sensor networks," *IEEE Wirel. Commun.*, vol. 24, no. 5, pp. 143–149, 2017.

[24] S. Pan, M. Lin, M. Xu, S. Zhu, L.-A. Bian, and G. Li, "A low-profile programmable beam scanning holographic array antenna without phase shifters," *IEEE Internet Things J.*, 2021.

[25] Q.-D. Cao, X.-X. Yang, F. Yu, and S. Gao, "High Scanning Rate Millimeter Wave Circularly Polarized CTS Leaky-Wave Antenna," *IEEE Trans. Antennas Propag.*, 2024.

[26] Y. Wang, Z. Zhang, and H. Li, "Universal quickest sensing of spectrum change in millimeter wave communications: a data driven approach," in *GLOBECOM 2017-2017 IEEE Global Communications Conference*, 2017, pp. 1–6.

[27] Z. Zhang, L. Li, Y. Fan, and H. Li, "Object tracking via blocking in millimeter wave communications: A blessing misfortune," in *2018 IEEE International Conference on Communications (ICC)*, 2018, pp. 1–6.

[28] L. K. Mathew, S. C. Nagavarapu, and A. Abraham, "Design and implementation of a Joint Sensing & Communication System for Connected Autonomous Vehicles," in *2022 17th International Conference on Control, Automation, Robotics and Vision (ICARCV)*, 2022, pp. 392–396.

[29] P. Zetterberg and R. Fardi, "Open source SDR frontend and measurements for 60-GHz wireless experimentation," *IEEE Access*, vol. 3, pp. 445–456, 2015.